Available online at www.sciencedirect.com
SCIENCE DIRECT®
ELSEVIER
International Journal of Solids and Structures 43 (2006) 2441–2459
INTERNATIONAL JOURNAL OF SOLIDS and STRUCTURES
www.elsevier.com/locate/ijsolstr

Evaluation of the stress–strain curve of metallic materials by spherical indentation

M. Beghini [a,*], L. Bertini [a], V. Fontanari [b]

[a] Dpt. Ingegneria meccanica, nucleare e della produzione, University of Pisa, Via Diotisalvi, 2, 56126 Pisa, Italy
[b] Dpt. Ingegneria dei materiali e tecnologie industriali, University of Trento, via Mesiano, 7, 38050, Italy

Received 10 January 2005; received in revised form 14 June 2005
Available online 12 September 2005

Abstract

A method for deducing the stress–strain uniaxial properties of metallic materials from instrumented spherical indentation is presented along with an experimental verification.

An extensive finite element parametric analysis of the spherical indentation was performed in order to generate a database of load vs. depth of penetration curves for classes of materials selected in order to represent the metals commonly employed in structural applications. The stress–strain curves of the materials were represented with three parameters: the Young modulus for the elastic regime, the stress of proportionality limit and the strain-hardening coefficient for the elastic–plastic regime.

The indentation curves simulated by the finite element analyses were fitted in order to obtain a continuous function which can produce accurate load vs. depth curves for any combination of the constitutive elastic–plastic parameters. On the basis of this continuous function, an optimization algorithm was then employed to deduce the material elastic–plastic parameters and the related stress–strain curve when the measured load vs. depth curve is available by an instrumented spherical indentation test.

The proposed method was verified by comparing the predicted stress–strain curves with those directly measured for several metallic alloys having different mechanical properties.

This result confirms the possibility to deduce the complete stress–strain curve of a metal alloy with good accuracy by a properly conducted instrumented spherical indentation test and a suitable interpretation technique of the measured quantities.

Keywords: Spherical indentation; Strain hardening; Yield strength; Stress–strain curve

* Corresponding author. Tel.: +39 050 836616; fax: +39 050 836665.
E-mail address: beghini@ing.unipi.it (M. Beghini).

0020-7683/$ - see front matter © 2005 Elsevier Ltd. All rights reserved.
doi:10.1016/j.ijsolstr.2005.06.068

1. Introduction

Indentation tests have been extensively employed in order to measure technological characteristics and to estimate mechanical properties of materials. In particular, the hardness is obtained by dividing the maximum force applied during the indentation by the extension of the residual crater produced on the surface of the sample. The relatively simple and low-cost procedure, the possibility to be applied on a small sample and the characteristic to be a non-destructive test applicable also on in-service components, are some reasons for the diffusion of the hardness test for material qualification.

Several empirical relationships have been proposed for directly correlating hardness with yield and tensile strengths (Tabor, 1951; Shabel and Young, 1987; Lai and Lim, 1991; Fischer-Cripps, 2000). Unfortunately, those empirical relationships are valid only for specific classes of materials and this makes the use of the hardness properties a procedure not much accurate and not general to evaluate the main material strength parameters.

The introduction of the instrumented indentation testing machines made many details of the indentation process to be available and stimulated a great effort to develop more refined procedures (e.g., Johnson, 1985; Au et al., 1980; Taljat et al., 1998; Giannakopoulos and Suresh, 1999; Nayebi et al., 2001) for getting more accurate estimates of the elastic–plastic properties.

The instrumented indentation test can produce an accurate and complete sampling of the load (L) vs. penetration depth (h) curve (hereafter called L–h curve). The L–h curve depends on several physical properties of the tests but it is mainly affected by the uniaxial stress–strain (σ–ε) curve of the sample material. Unfortunately, this dependence is not so simple to be predicted, mainly as a consequence of the complexity of the deformation process produced in the indentation region. Indeed, in the indentation region the material of the sample exhibits multiaxial stress conditions with high gradients and large elastic–plastic strains. Strong non-linearities are also induced by the unilateral contact and the involved large displacements.

Some authors (e.g., Fischer-Cripps, 1997, 2000; Taljat et al., 1998; Giannakopoulos and Suresh, 1999; Hill et al., 1989) used the slope of the L–h curve produced during loading to estimate plastic flow properties and deduced the Young modulus by the slope during unloading (Rickerby, 1982; Pharr and Oliver, 1992; Pharr et al., 1992; Huber et al., 1997; Fischer-Cripps, 2000; Nayebi et al., 2002).

In a pioneering work of the spherical indentation, on the basis of experimental results, Meyer (1908) proposed an empirical power relationship correlating the load to the diameter (d) of the crater:

$$L = B \cdot d^{\mu} \tag{1}$$

where B and μ are material properties. Successively, Tabor (1951) found that the Meyer's exponent μ can be related to the strain-hardening exponent m, used to define the true stress–true strain curve in the plastic region by means of a power law relationship ($\sigma = K\varepsilon^m$). The following simple empirical relationship:

$$m = \mu - 2 \tag{2}$$

was found to be reasonably accurate for many materials, if the applied load is high enough to generate a fully plastic enclave around the contact region.

Tabor presented a complete physical description of the material deformation during the indentation process. Assuming that the material embedding the indenter is completely in the plastic regime, Tabor obtained a correlation between the stress–strain curve and the indentation parameters: the crater diameter (d), the indenter diameter (D) and the applied load (L).

On the basis of an extensive analysis of experimental results found in the literature, Francis (1976) generalized and improved the Tabor's model by subdividing the indentation process in three stages: elastic, transition and fully plastic. Other authors (Au et al., 1980; Johnson, 1985; Tirupataiah and Sundararajan, 1991; Taljat et al., 1998; Giannakopoulos and Suresh, 1999; Beghini et al., 2002) contributed to refine and extend the Tabor approach, particularly analyzing the effect of the indenter shape.

Norbury and Samuel (1928) observed non-negligible differences between the shape of the crater measured after testing and that predicted by geometrical considerations based on the assumptions of perfectly rigid indenter and rigid-perfectly plastic target material. In particular, they showed that some materials flow at the crater boundary thus producing a ridge over the level of the undeformed surface ('piling-up' phenomenon). Other materials exhibit the 'sinking-in' phenomenon in which the residual crater has a smoother edge, and the deformed surface is completely under the level of the undeformed surface. It was observed that this difference is related to the material plastic flow characteristic: the piling-up is observed in low strain-hardening materials, the sinking-in in high strain-hardening materials.

Some authors (Fischer-Cripps, 1997, 2000; Taljat et al., 1998; Mesarovic and Fleck, 1999; Nayebi et al., 2001) observed that indentation phenomenon can be better modelled by the 'physical' crater diameter, representing the size of the region in contact with the indenter at the maximum load. The physical diameter can be significantly different from the 'geometrical' diameter that measures the extension of the final crater after the test, particularly for materials with high strain hardening. In fact, the accuracy of the Tabor model can be improved and its range of applicability extended if the 'geometrical' diameter is replaced by the 'physical' diameter. Unfortunately, it is not so simple to take a practical advantage from this fact. Indeed, the final geometrical diameter can be easily measured and its current value can be directly calculated during the test on the basis of the indentation depth, on the contrary the physical diameter (being affected by the unknown properties of the target material) cannot be obtained by direct elaboration of the measured quantities. Some authors (Matthews, 1980; Hill et al., 1989; Tirupataiah and Sundararajan, 1991; Taljat et al., 1998) suggested that the ratio between the physical and the geometrical diameters can be considered a function of the strain-hardening coefficient and the ratio between the yield strength and the Young modulus. On this hypothesis, a scaling approach was proposed to account for the variability of the yield stress (Fischer-Cripps, 1997; Taljat et al., 1998; Mesarovic and Fleck, 1999).

Taljat et al. (1998) observed that the local effective stress–strain curves calculated in particular positions in the crater region resemble the uniaxial stress–strain material curve. On this basis, an approximate procedure for deducing the strain hardening was developed that is valid only for a given ratio between yield strength and the Young modulus.

Recently, the authors (Beghini et al., 2002) performed an extensive parametrical finite element analysis of the spherical indentation in order to study the dependence of the crater shape to the yield stress and strain hardening. As a general result it was found that a direct correlation between the crater shape and the material properties is not evident. Indeed, unavoidable uncertainties arise when trying to separate the contact stages (elastic, mixed and fully plastic) and to reproduce the effective size and shape of the contact region.

In the authors' opinion, the methods proposed with the aim at improving the Tabor's approach for deducing the stress–strain curve, have reached their limits and it is difficult to find ways for making them more accurate and general. Those methods have lost the simplicity of the Tabor approach by introducing corrective functions, that make the interpretation of the measured quantities complex, indirect and sometimes questionable for the applicability at large classes of materials. Moreover, in some cases, the corrective functions lack of clear physical bases and they can introduce inaccuracies and biases, particularly during the inversion procedure (i.e., when from L–h the σ–ε curve is obtained).

For these reasons, the authors (Beghini et al., 2001) proposed a direct method for deducing the σ–ε curve of a material from load vs. displacement curves obtained in tests with similar characteristics. By applying this method to spherical indentation, any reference to the effective crater shape is avoided as only the quantities L and h are required in input.

An approach based on the direct correlation between the L–h curve and σ–ε curve was also applied by Nayebi et al. (2001) for characterizing surface structurally graded materials. After approximating the L–h curve by a polynomial and applying an optimization technique, the yield stress and the strain-hardening coefficient were deduced by a best fit procedure. The method was applied to different materials with a maximum error of 25% in the yield strength and 20% in the strain-hardening coefficient.

In the present paper a general direct method is proposed for accurately determining the material uniaxial properties defining the σ–ε curve from the L–h curve measured in spherical indentation.

2. Proposed approach for evaluating the stress–strain curve by instrumented spherical indentation

The present study started by an extensive accurate finite element analysis of the indentation process aimed at determining the load vs. indentation depth (L–h) curves for different classes of materials. In order to have a parametric representation of the material uniaxial σ–ε curve, the following Hollomon like power law expression was assumed:

$$\sigma(\varepsilon) = \begin{cases} E \cdot \varepsilon, & \varepsilon \leqslant \dfrac{\sigma_0}{E} \\ \sigma_0^{(1-n)} \cdot E^n \cdot \varepsilon^n, & \varepsilon > \dfrac{\sigma_0}{E} \end{cases} \tag{3}$$

where E is the Young modulus, ε the total strain (elastic + plastic), n the strain-hardening coefficient and σ_0 proportionality limit stress.

By Eq. (3) any material is represented by three parameters: E, σ_0, n. The curve (3) is shown in Fig. 1, along with a corresponding typical measured σ–ε curve for a metal. The yield strength (σ_{ys}) measured on an experimental σ–ε curve is usually higher than σ_0. For this reason, the stress ($\sigma_{y0.2}$) corresponding to a plastic strain of 0.2% ($\varepsilon = 0.002 + \sigma_{y0.2}/E$ in Eq. (3)), was defined as an estimate of the yield strength by Eq. (3). It has to be observed that, in a real material, different definitions of the yield strength σ_{ys} can be applied, in dependence of the local shape of the measured σ–ε curve at yielding.

The use of Eq. (3) is somewhat arbitrary, however, the method proposed in the present paper is general and no theoretical limit exists for its extension to other representations of the σ–ε material curve (for instance a bilinear curve).

Several combinations of the material parameters (E, σ_0 and n) were taken into account in order to map a domain wide enough to cover the properties of the most common metallic materials used in structural applications.

As a result of this analysis, a database of FE simulated L–h curves for a wide range of target materials was obtained (hereafter indicated as $L^{(FE)}$–$h^{(FE)}$ curve). No preliminary assumption was made on the shape

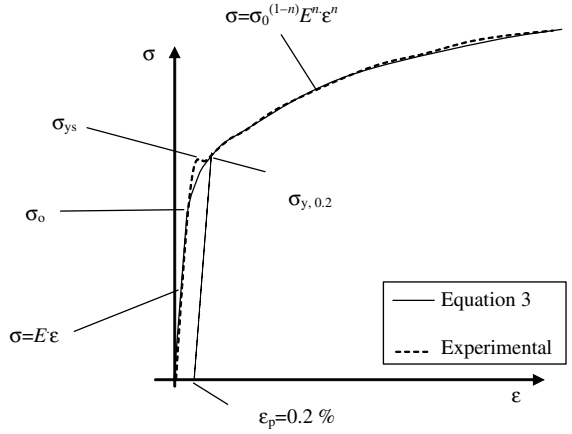

Fig. 1. Representation of the fitting parameters of Eq. (3).

of the $L^{(FE)}$–$h^{(FE)}$ curves, and they where stored in the database as the complete sequence of the effectively calculated pairs ($L^{(FE)}$, $h^{(FE)}$) for any combination of material parameters.

The analysis of the whole database of simulated $L^{(FE)}$–$h^{(FE)}$ values, indicated that, within any class of alloy (defined by the value of E), each curve could be accurately fitted by a properly chosen three-terms power expansion. The coefficients of the power expansions were then expressed as functions of the other material parameters (σ_0 and n). As a preliminary result, a completely analytical expression was obtained for any class of material that gives a 'theoretical' L–h curve (hereafter called $L^{(th)}$–$h^{(th)}$ curve) by any couple of values σ_0 and n in the analyzed domain.

In the following, the procedure for obtaining the $L^{(th)}$–$h^{(th)}$ curve on the basis of any combination of σ_0 and n for any class of material is called direct procedure.

By adopting an optimization algorithm, the direct procedure was then inverted, thus allowing the parameters (σ_0 and n) of the material stress–strain curve to be deduced by a given sequence of experimentally obtained L–h values ($L^{(exp)}$–$h^{(exp)}$). This is called the inverse procedure. The final results is the σ–ε curve represented by Eq. (3) by which the given indentation curve is reproduced at best on the basis of a proper matching criterion.

The direct and the inverse procedures were validated by comparing their results to independent FE simulations showing a general very good agreement. Moreover, several verifications were performed by using experimental values obtained with different materials. The final section gives a quantitative assessment of the obtained accuracy.

3. Finite element analysis of the indentation process

3.1. FE model

The FE simulation of the spherical indentation was carried out with the Ansys Rel. 5.6 computer program. Due to the axi-symmetrical geometry, a two-dimensional model was generated, whose characteristics were defined on the basis of several preliminary analyses which indicated that:

(1) In spite of the generally adopted assumption for sharp indenters (Johnson, 1985; Giannakopoulos and Suresh, 1999; Fischer-Cripps, 2000), the spherical indenter cannot be modelled as a rigid body. Indeed, particularly for target materials with high σ_0 or n, the contribution of the indenter deformation to the size and shape of the crater cannot be neglected. According to Field and Swain (1993) and Taljat et al. (1998), an elastic indenter (having diameter $D = 2$ mm) made by tungsten–carbide ($E_{ind} = 534$ GPa, $\nu_{ind} = 0.22$) was modelled.
(2) As observed also by Taljat et al. (1998) and Herbert et al. (2001), friction in the contact region was found to produce negligible effects on the L–h curve, whereas it affects the stress distribution beneath the indenter. Consequently, in order to reduce the elaboration time and facilitate the convergence, frictionless point to surface gap elements (Ansys contact 48) were adopted.
(3) The stress–strain field exhibits a complex distribution in a small region around the crater. In order to avoid the influence of the finite model dimensions on the solution, the target material was modelled as a cylinder having diameter $D_m = 5D$ and height $H_m = 10D$. With this choice, the presence of the stress-free surfaces (excluding the upper surface) affects the local stress within 0.5%. Similar model dimensions were also assumed by Fischer-Cripps (1997).

The mesh in the indentation region was refined by comparing the numerical solution with the Hertzian analytical solution for the elastic contact. The stress was reproduced with a maximum relative error of 1.5% and the maximum indentation depth with an error of 0.1% at the onset of plasticity in the target material.

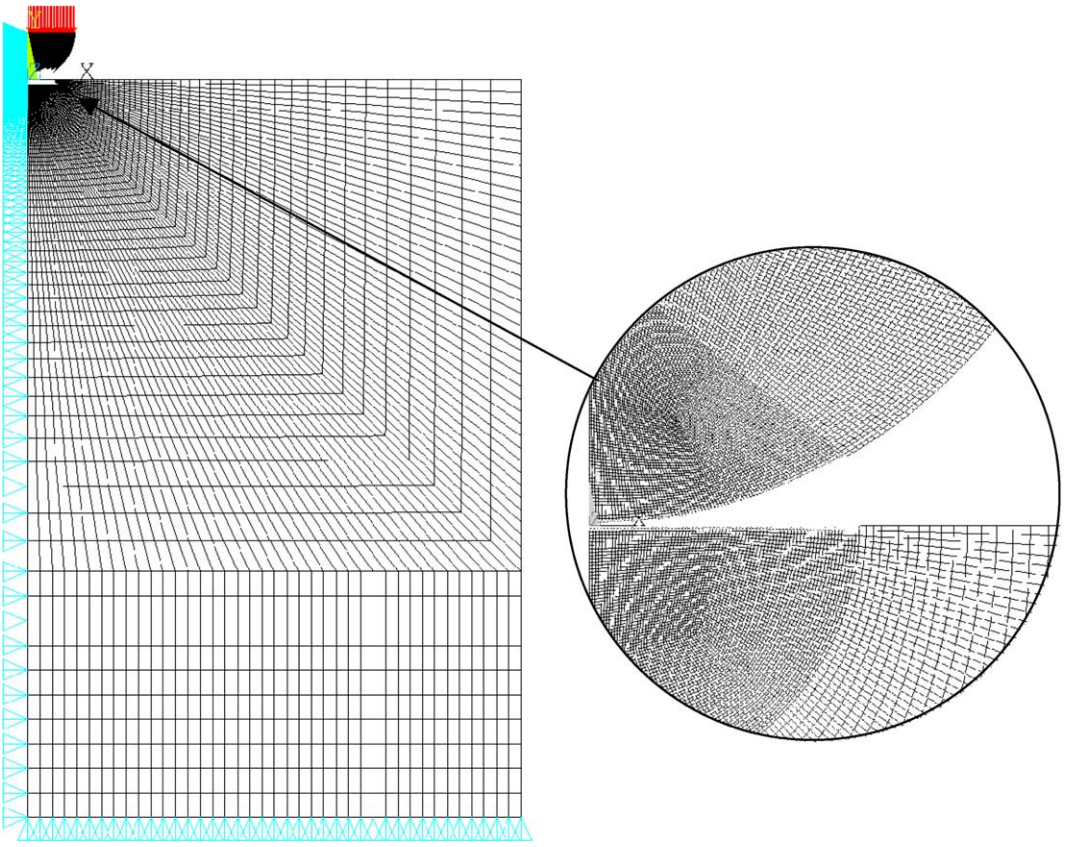

Fig. 2. Finite element model used for the analysis.

As no reference solution can be found in the elastic–plastic regime, it was not possible to assess the solution at higher loads. However, as the plasticity tends to reduce the stress gradients, it is expected that the numerical simulation of the phenomenon has comparable accuracy also in the elastic–plastic regime.

The final FE model, shown in Fig. 2, was made by nearly 20,000 eight-node isoparametric elements (Ansys stiff 82) and nearly 1200 point to surface gap elements (Ansys contact 48). The elements in the contact region have a characteristic dimension $a = 6$ μm ($a/D = 3 \times 10^{-3}$).

3.2. Experimental verification of the FE simulation

The aim of the FE analysis was to build up a database of $L^{(FE)}$–$h^{(FE)}$ curves. The FE analyses were considered ideal instrumented spherical indentations that eliminated the difficulties and the cost of a complete sampling of the domain by extensive experimental tests. In order to assess the accuracy of the FE simulation of the phenomenon, several tests were carried out for comparison.

The tests were conducted on six different materials. The average values and the scatter ranges (±3 standard deviation) of the material properties determined on the basis of five uniaxial tensile tests for any material are reported in Table 1.

The true stress–true strain values were fitted with the expression (Eq. (3)) by means of a non-linear least square fitting procedure. The obtained Hollomon curves compared with the experimental results are shown in Fig. 3, whereas the relevant material parameters are reported in Table 2.

Table 1
Tensile properties of the studied materials, mean value and three standard deviations: Young modulus, yield strength, ultimate strength, maximum total strain

	E (GPa)	$\sigma_{y,0.2}$ (MPa)	σ_r (MPa)	A (%)
C40	211 (±2)	412 (±4)	865 (±14.2)	16.2 (±1.5)
AISI 316L	180 (±4)	297 (±5)	864 (±11.5)	34.5 (±2.0)
Cu (work hardened)	121 (±4)	254 (±2)	283 (±2.1)	12.6 (±1.4)
Cu (annealed)	117 (±4)	55 (±2)	313 (±5.1)	36.3 (±1.6)
6060 Al-alloy	74 (±3)	302 (±4)	355 (±4.5)	8.4 (±1.6)
7075 Al-alloy	72 (±3)	534 (±5)	635 (±4.8)	12.1 (±1.9)

The values of the scatter s and of the correlation coefficient R are defined by the following expressions:

$$s = \sqrt{\frac{\sum_{i=1}^{N}\left(\sigma_i^{(\text{Eq. (3)})} - \sigma_i^{(\text{exp})}\right)^2}{N-1}}, \qquad R^2 = \frac{\sum_{i=1}^{N}\left(\sigma_i^{(\text{Eq. (3)})} - \sigma_{\text{average}}^{(\text{Eq. (3)})}\right)^2}{\sum_{i=1}^{N}\left(\sigma_i^{(\text{exp})} - \sigma_{\text{average}}^{(\text{exp})}\right)^2} \quad \text{and} \quad \sigma_{\text{average}} = \frac{\sum_{i=1}^{N}\sigma_i}{N} \tag{4}$$

where N is the number of measured couples (for any material) and the superscripts indicate the origin of the relevant quantities. These values were included in Table 2 to indicate the ability of the Hollomon curve (3) to directly reproduce the measured curves for the different classes of materials. It can be noted that the calculated Hollomon stress–strain curves reproduce the experimental curves with an acceptable accuracy in a wide strain range for any tested material.

A device for the spherical indentation was set up on a servo-hydraulic testing machine. The relative displacement between indenter and target was measured by a LVDT transducer having an accuracy of 1 μm. A calibration procedure was carried out to determine the compliance of the testing apparatus. To this purpose, an elastic indentation on a WC–Co target material was performed and the measured indentation curve was compared with the theoretical curve for an elastic indentation. As a result, a Δh vs. L curve was determined to be used for correcting the displacements measured by the LVDT transducer during the indentation tests.

At least five complete indentation tests were carried out for each target material in displacement control at a speed of 0.05 mm/min.

The measured $L^{(\text{exp})}$–$h^{(\text{exp})}$ curves (properly corrected with the testing apparatus compliance) were compared with simulated $L^{(\text{FE})}$–$h^{(\text{FE})}$ curves obtained by introducing in the FE analysis the Hollomon curve directly fitted on the measured σ–ε points. The indentation pressure L/D^2 was plotted vs. the dimensionless depth h/D after introducing, as a scaling factor, the indented diameter D as the characteristic length of the problem.

As shown in Fig. 4, the experimental and the FE simulated L–h indentation curves are in a fairly good agreement, thus demonstrating the capability of the FE model of simulating the indentation process with a satisfactory accuracy.

Two examples of simulated indentation craters are compared with the corresponding residual craters measured by a profilometer in Fig. 5. It is worth noting that piling-up was predicted and effectively observed for a low strain-hardening material (Al–Mg alloy with $n = 0.06$) while sinking-in was predicted and observed for a strain-hardening material (AISI 316L with $n = 0.28$).

3.3. Parametric analysis of the $L^{(FE)}$–$h^{(FE)}$ curves

The agreement between the experimental and the numerical results confirmed the possibility of building up, by a parametric FE analysis, an accurate and extensive database of L–h curves for different materials with E, σ_0 and n varying in wide ranges.

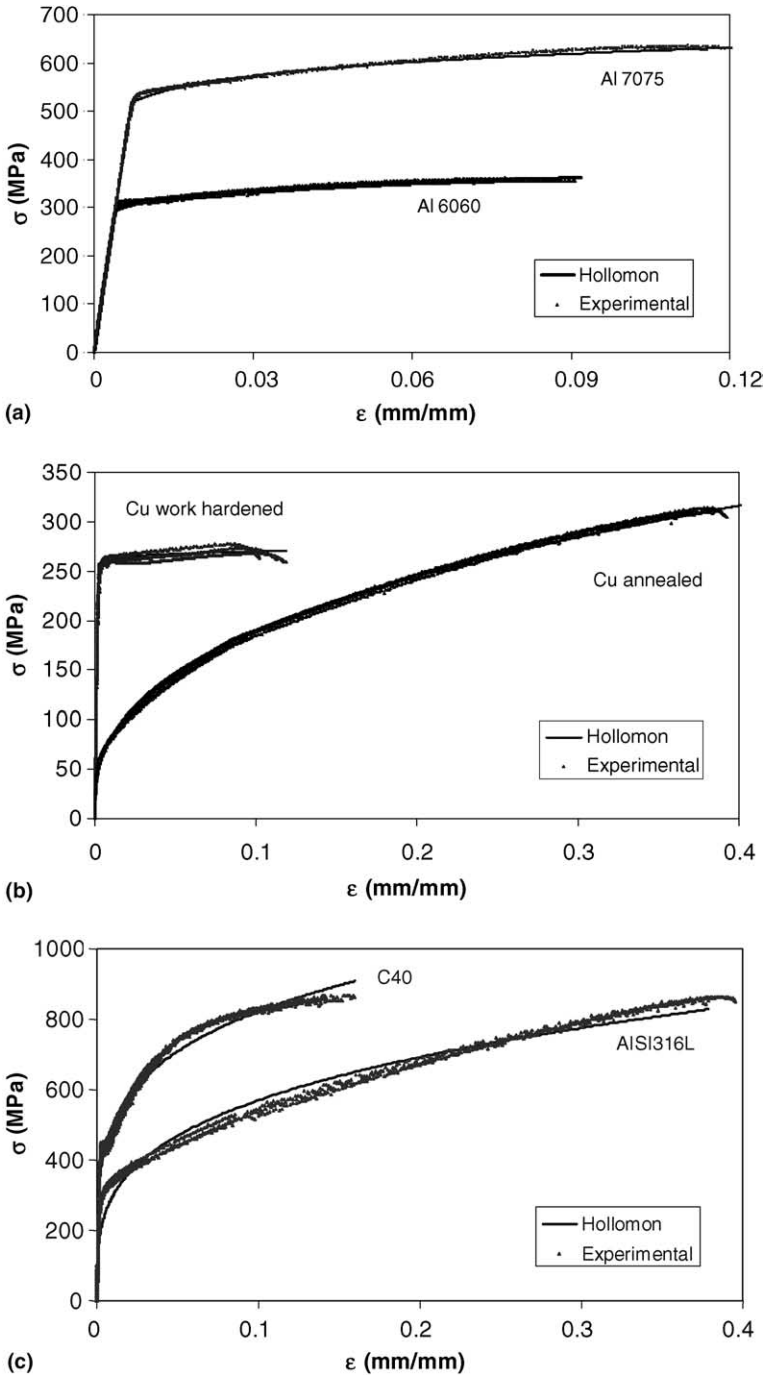

Fig. 3. Comparison between experimental σ–ε curves and the best fitting curves based on Hollomon's law.

Three classes of metallic alloys were considered: Al-alloys characterized by a Young modulus $E = 70$ GPa, the Cu-alloys ($E = 120$ GPa) and the steels ($E = 205$ GPa). As the Young modulus can be

Table 2
Parameters of the fitting curves obtained by Eq. (3)

	E (GPa)	σ_0 (MPa)	$\sigma_{y,0.2}$ (MPa)	n	s	R^2
C40	211	344	415	0.215	20.14	0.968
AISI 316L	180	148	220	0.278	25.07	0.978
Cu (work hardened)	121	251	255	0.013	4.49	0.991
Cu (annealed)	117	17.5	48	0.368	4.18	0.995
6060 Al-alloy	74	295	301	0.061	5.07	0.971
7075 Al-alloy	72	520	527	0.071	4.53	0.986

considered approximately a constant parameter within each class of materials, and the Poisson ratio is near 0.3 for almost all metals, within any class, the constitutive parameters were reduced to the proportional stress σ_0 and the strain-hardening coefficient n.

A set of σ–ε curves was generated by using Eq. (3) in order to represent a wide range of elastic plastic material properties. For steel alloys, σ_0 was chosen in the range $100 \leqslant \sigma_0 \leqslant 1000$ MPa with a step of 100 MPa, and the strain-hardening coefficient n in the range from 0.0 to 0.5 with a step of 0.05. For both Al-alloys and Cu-alloys, σ_0 was chosen in the range $60 \leqslant \sigma_0 \leqslant 660$ MPa with a step of 60 MPa, and n in the range $0 \leqslant n \leqslant 0.48$ with a step of 0.06.

In the FE analyses, the Hollomon curves were approximated by a piecewise multilinear function with strain intervals varying along the curve in order to limit the introduced error in the σ estimation within 1% along the complete σ–ε curve.

The plastic flow was modelled in the hypothesis of isotropic hardening, assuming the Von Mises multiaxial yielding criterion and the associated Prandtl–Reuss plastic flow rule. Indentations were simulated by a multistep loading sequence up to a maximum nominal pressures $L/D^2 = 250$ MPa for steels and 200 MPa for either Al-alloys or Cu-alloys.

The load was applied as a uniform pressure on the equatorial plane of the spherical indenter (Fig. 2). Some of the simulations for materials having low yield strength and low strain hardening were stopped at lower nominal pressures due non-convergence.

An example of the effect produced by the material parameters on the simulated $L^{(\mathrm{FE})}$–$h^{(\mathrm{FE})}$ curves can be observed in Fig. 6.

3.4. Analysis of the independent parameters

Some authors (Hill et al., 1989; Mesarovic and Fleck, 1999; Taljat et al., 1998) suggested the possibility to simplify the analysis by normalizing the nominal pressure with the material yield strength, thus reducing the number of independent physical variables. On the basis of this approach, the strain-hardening coefficients n should become the only material parameter effectively affecting the solution.

The availability of a so large amount of results made it possible to verify that proposal. As an example, several curves for different σ_0 are plotted for the same strain-hardening coefficient in Fig. 7. By comparing Figs. 7 and 6(c), a tendency of the curves to converge to a unique 'master' curve (one for each n) when the nominal pressure is normalized by σ_0 can be observed. However, the convergence is not complete and the points show a non-negligible scatter that tends to increase for larger strain-hardening coefficients.

This observation seems to suggest that the proposed normalization is not suitable for obtaining accurate correlation between σ–ε and L–h curves.

A physical explanation for the impossibility to obtain a model depending on a unique parameter can be found. The proposed normalization would produce a unique master curve if the crater shape (and in particular its depth h) were produced by the plastic strains only (which are functions of the plastic properties σ_0 and n). However, a contribution is given also by the elastic strains, either under load or after the load

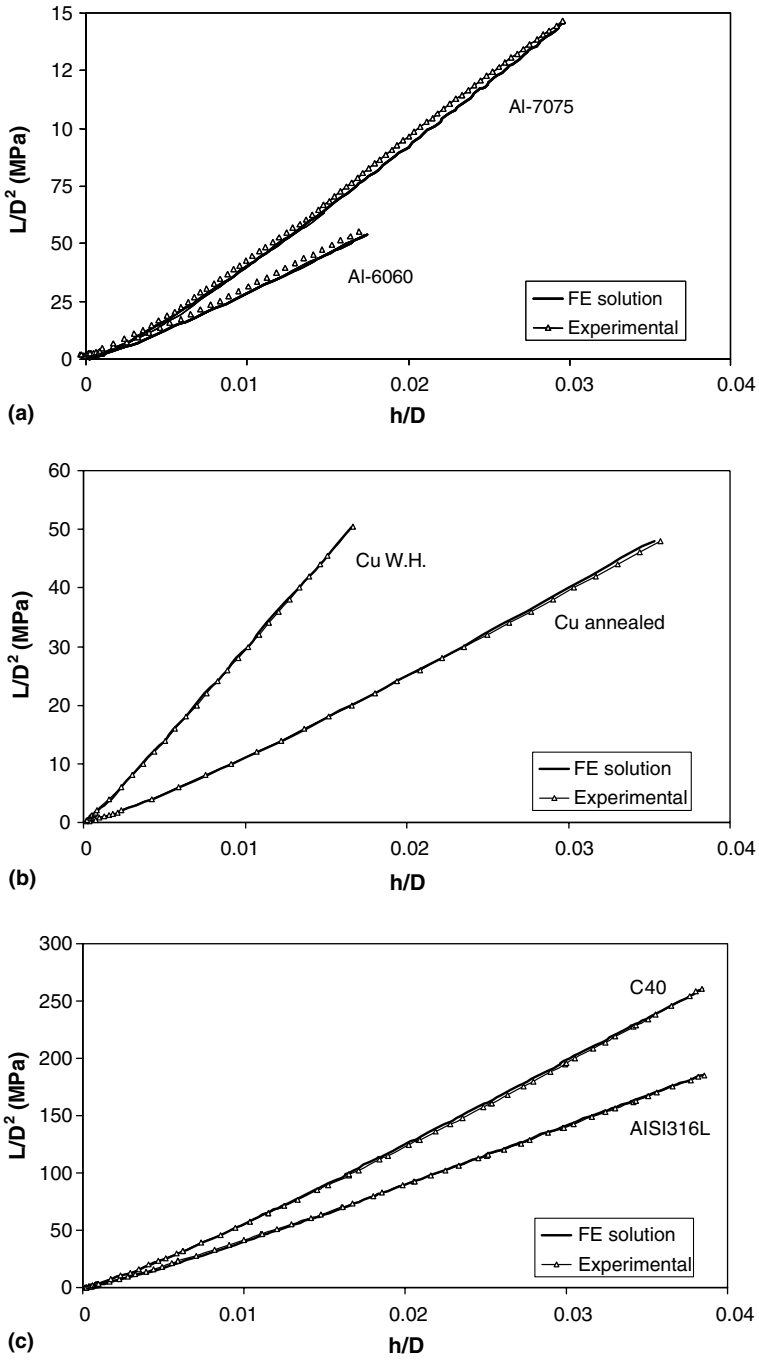

Fig. 4. Numerical and experimental indentation curves for the investigated materials.

removal. Indeed, also after the indenter is removed, a non-negligible residual stress field (with the related elastic strains) is present in the target material.

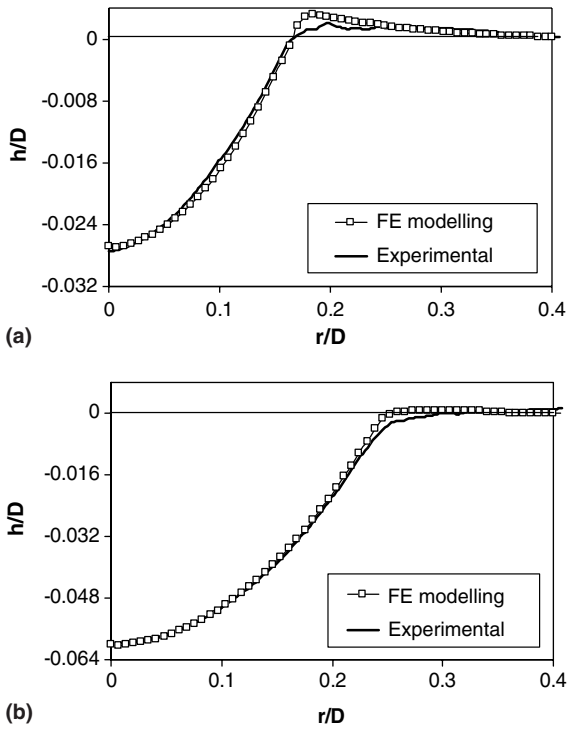

Fig. 5. Residual indentation profiles obtained by FE and measured after experiments: (a) Al–Mg alloy, (b) AISI316L.

This conclusion is supported by the evidence that the normalized points shows less scatter around the 'master curve' for materials with low strain hardening and yield strength.

If the elastic strains are considered, the Young modulus should be included in the dimensional analysis. For this reason the independent dimensionless quantities can be effectively reduced from three to two (for instance: n and σ_0/E). A unique dimensionless 'master surface' with two parameters could be determined thus including both elastic and plastic strains. However, this solution was not taken into account in the present study by considering that, in practice, the Young modulus is not a continuous parameter as it is almost constant within the classes of materials herein considered.

4. Interpolation of the L–h curves: direct procedure

4.1. Evaluation of the theoretical L–h function

A least square fitting of the $L^{(FE)}$–$h^{(FE)}$ curves obtained by the parametrical simulation was carried out by adopting the following expansions (Beghini et al., 2001):

$$\frac{L}{E \cdot D^2} = \sum_{k=1}^{4} A_k \cdot \left(\frac{h}{D}\right)^{k/2} \tag{5}$$

These functions were preferred to the polynomials with integer exponents (Nayebi et al., 2002), as higher correlations can be obtained in the whole database range.

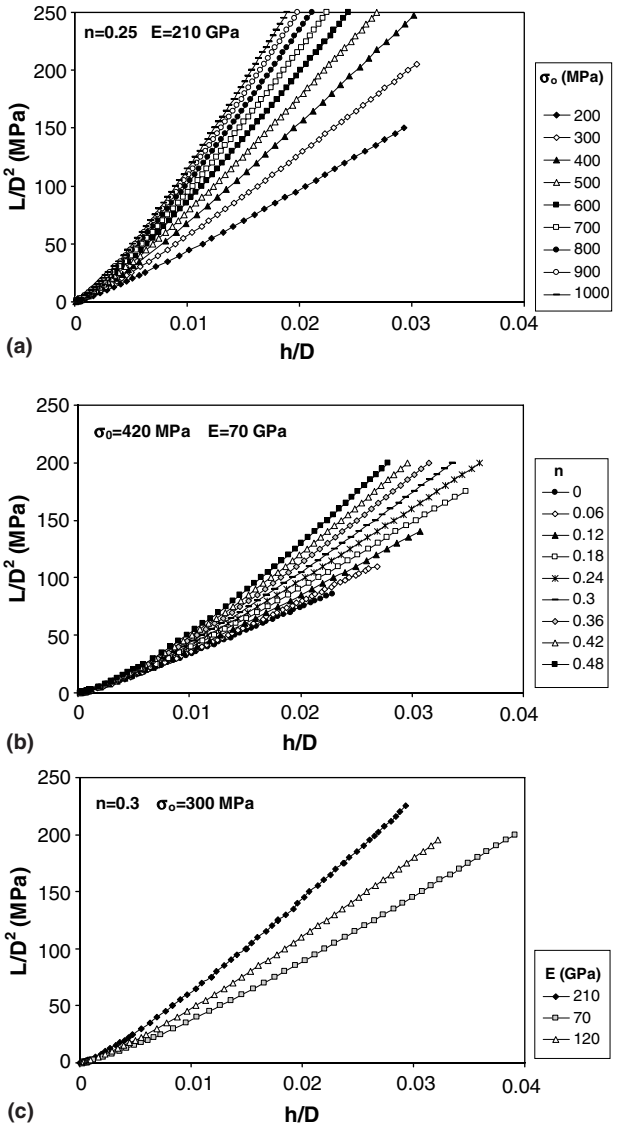

Fig. 6. Effect of different parameters on L–h curves: (a) varying σ_0 (E, n constant), (b) varying n (E, σ_0 constant), (c) varying E (n, σ_0 constant).

For different classes of elastic properties, the best fitting coefficients A_k were calculated for any combination of the parameter σ_0 and n used in the database creation, thus obtaining a sampling of the following two-dimensional functions:

$$A_k = A_k(\sigma_0, n), \quad k = 1, 2, 3, 4 \tag{6}$$

A two-dimensional polynomial function was introduced (one for any A_k and any class of elastic properties) to fit these values:

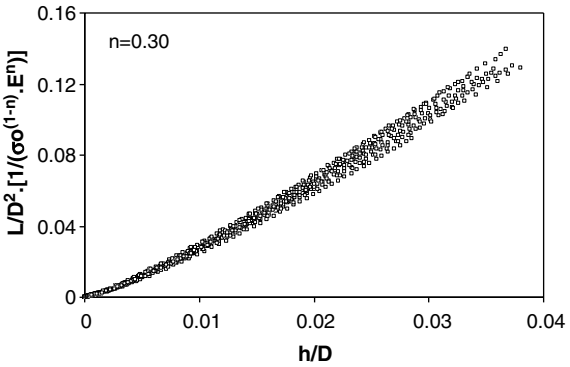

Fig. 7. Non-dimensional curves for materials with $n = 0.3$ and different E and σ_0.

$$A_k = \sum_{i=1}^{6}\sum_{j=1}^{6} \alpha_{ijk} \cdot \sigma_0^{i-1} \cdot n^{j-1} \tag{7}$$

by means of the least squared fitting method.

The three sets of 144 constant coefficients α_{ijk} (one set for any class of materials) so determined embody the whole database.

By using the expressions (5)–(7) the direct procedure is complete, as the theoretical $L^{(\mathrm{th})}$–$h^{(\mathrm{th})}$ curve can be analytically expressed for any class of material in the analyzed range by the following equation:

$$L^{(\mathrm{th})}(h, E, \sigma_0, n) = E \cdot D^2 \sum_{k=1}^{4}\sum_{i=1}^{6}\sum_{j=1}^{6} \alpha_{ijk} \cdot \sigma_0^{i-1} \cdot n^{j-1} \cdot \left(\frac{h}{D}\right)^{k/2} \tag{8}$$

in which the dependence of the load to the variable h and the material parameters has been explicitated.

It is worth noting that, in the present analysis, the $L^{(\mathrm{th})}$ functions were obtained for L/D^2 values not exceeding 250 MPa for steels and 200 MPa for the other alloys. Beyond these limits, the values obtained by the theoretical functions have to be considered an extrapolation of the simulated results and the accuracy of the predictions, hereafter quantified, is not guaranteed.

4.2. Verification of the theoretical L–h function

Several checks were set up in order to assess the validity of Eq. (8) and, consequently the accuracy of the direct procedure by which the L–h curve can be predicted on the basis of the material properties. To this purpose, all the materials used in the experimental verification were considered. In Fig. 8, indentation (L–h) curves obtained by:

- points deduced by FE modelling with the material elastic–plastic properties measured by the tensile tests: $L^{(\mathrm{FE})}$–$h^{(\mathrm{FE})}$ (curves labelled with FEM);
- points directly obtained by indentation tests: $L^{(\mathrm{exp})}$–$h^{(\mathrm{exp})}$ (curves labelled with experimental);
- points calculated by applying the direct procedure (Eq. (8)) by using the material parameters E, σ_0 and n of Table 2 fitted on the measured σ–ε curves (curves labelled with calculated);

are compared.

It can be observed that, within the domain of analysis, the points are reproduced by Eq. (8) with a relative error not exceeding 1%. This result was considered a confirmation of the capability of the direct

procedure to accurately predict the L–h curve when the elastic–plastic properties are known and the σ–ε curve can be reasonably represented by the three parametrical equations (3).

The α_{ijk} values obtained for the three classes of materials are not reported for brevity. However, the authors can provide the A_k coefficients on request if the material uniaxial properties are given (for instance by E-mail).

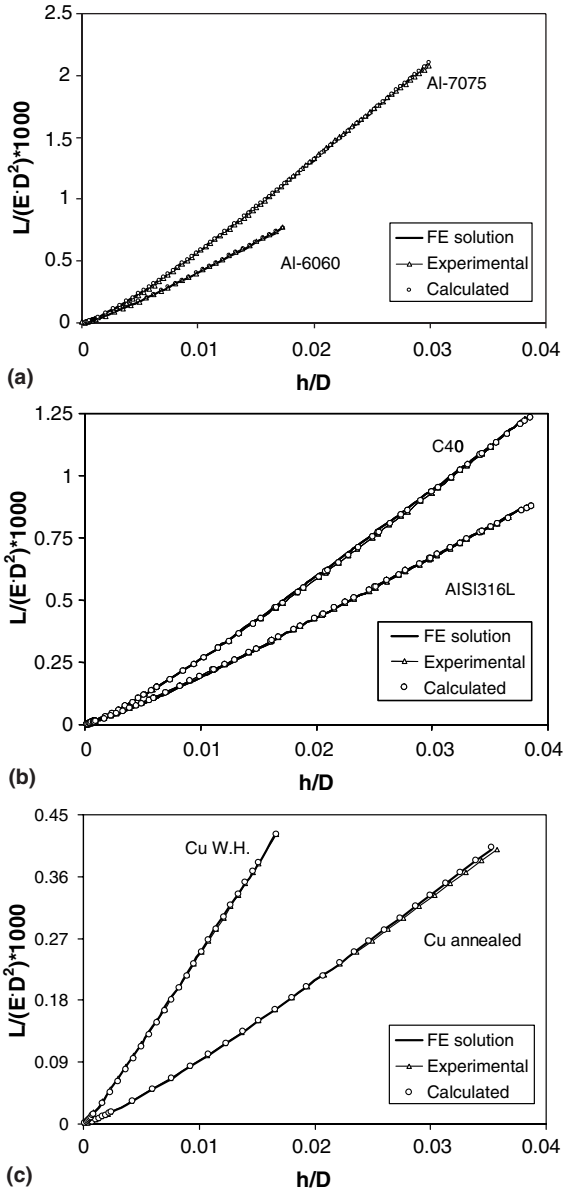

Fig. 8. Comparison between the L–h curves calculated by Eq. (4) with those determined experimentally and by FE.

5. Deduction of the σ–ε curves from instrumented indentation test: inverse procedure

5.1. Method for deducing the σ–ε curve

As demonstrated in the previous section, the direct procedure represents a rapid method for determining the L–h curve when the material properties are known. In this section the inverse procedure is described, that is the method for determining the material parameters σ_0 and n by the measured $L^{(\exp)}$–$h^{(\exp)}$ curve.

A direct analytical evaluation of the stress–strain curve starting from a given L–h curve was not possible. For this reason a numerical method based on an optimization algorithm was used.

The typical output obtainable from an instrumented indentation test is not a continuous function but a sequence of M couples of measured values $L_m^{(\exp)} - h_m^{(\exp)}$ with $m = 1, \ldots, M$. By adopting modern acquisition systems, M can be a relatively large number in the order of 100 or more, thus the experimental indentation curve can be adequately represented by the sequence of couples.

It must considered that the M couples are also affected by experimental errors which are usually difficult to predict. If we assume that any reasonable source of bias has been eliminated, the experimental points are affected by the typical scatter due to random errors. As a consequence, a rational method for interpreting these data is to find a L–h curve which fits the points within the level of the random error.

To this purpose the following function $\chi(E, \sigma_0, n)$ was introduced:

$$\chi(E, \sigma_0, n) = \sum_{m=1}^{M} \left[L^{(\mathrm{th})}\left(h_m^{(\exp)}, E, \sigma_0, n\right) - L_m^{(\exp)} \right]^2 \tag{9}$$

that can be considered a measure of the global distance between the measured points $L_m^{(\exp)}$–$h_m^{(\exp)}$ and a theoretical curve defined by the material properties (E, σ_0, n).

The procedure requires the knowledge of the class of material, in order to set the parameter E in relationship (9). From this starting point, an optimization algorithm (Beghini et al., 2001) scans the domain of the other material properties (σ_0, n), and by several applications of the direct procedure, selects the theoretical curve which minimize the function $\chi(E, \sigma_0, n)$.

The convexity of the function $\chi(E, \sigma_0, n)$ guarantees that the minimum exists and the minimization algorithms demonstrated to converge rapidly to the solution for any considered set of experimental points.

In order to verify the convergence of the optimization algorithm and its coherence, the inverse procedure was applied by assuming as input points the values simulated by the FE method for producing the database. The results of this self-consistency test are shown in Fig. 9. It can be observed that the inverse procedure finds the material properties with a fairly good accuracy as the relative errors are within 4% for σ_0 and within 2% for n in the whole ranges for any material class.

5.2. Experimental verification

To test the validity of the whole method, the experimental points obtained by spherical indentation tests were used as input of the inverse procedure. As an example, in Fig. 10 three σ–ε curves are compared:

- The curve obtained by Eq. (3) using as parameters the values determined by the direct least squared fitting of the σ–ε points measured in tensile tests (values in Table 2) (curve-labelled with Hollomon).
- The σ–ε points directly measured in tensile tests (curve-labelled with Experimental).
- The curve obtained by Eq. (3) using as parameters the values obtained by the inverse procedure applied to the values $L^{(\exp)}$–$h^{(\exp)}$ measured in indentation tests (curve-labelled with Calculated).

It can be observed that the calculated σ–ε curves approximate the experimental values with an accuracy comparable to that obtainable by a direct fitting with the Hollomon's law. The relative differences between

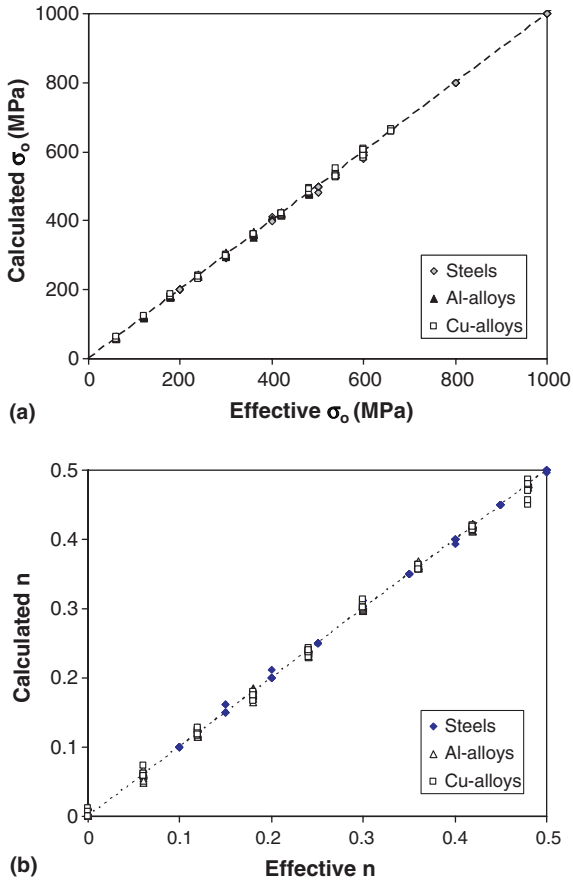

Fig. 9. Effective and calculated values of σ_0 (a) and the hardening exponent n (b).

the calculated and the fitted Hollomon's curves, are within a range of 4% for materials having rather different properties in a wide range. This level of accuracy is usually adequate in practical applications.

The maximum differences between Calculated and Experimental curves are located at the highest strain, while the agreement is very good in the near yield region. This can be considered as a consequence of the nature of the measured depth h. Indeed, the penetration depth is an integrated effect of the strains (mainly plastic) experienced by a finite region of material and, in that region, only a small portion reaches the extreme strain levels. For this reason, the procedure gives the best prediction in the range of small and average strain while it tends to extrapolate the values at the highest strain levels.

5.3. Practical application of the method

By the proposed method, an approximate σ–ε curve can be obtained under the following hypotheses:

(1) the class of material is known, with the corresponding Young modulus;
(2) the stress–strain curve can be represented by the Hollomon like expression (3);
(3) the set of the coefficients A_k is available.

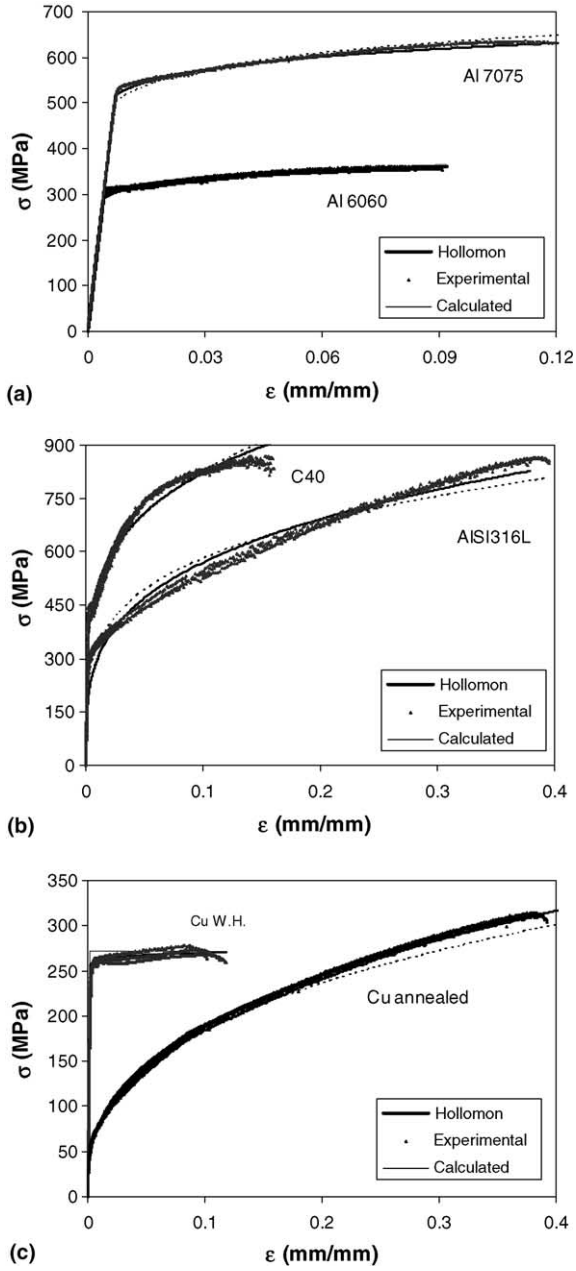

Fig. 10. Comparison between experimental, the calculated and the Hollomon σ–ε curves for the three classes of alloys used in the experimental characterization.

For the last point, any interested reader can contact the authors (for instance by E-mail) for obtaining the σ–ε curve by indicating the class of material and the sequence of appropriately measured $L_m^{(\exp)}$–$h_m^{(\exp)}$ values.

The method could seem not very general, as a consequence of the first two hypotheses. However, the case in which the Young modulus of a metallic material is completely unknown can be considered very rare.

Usually, the basic element of an alloy (which much affects the value of E) is well known while the uncertainties are related to the presence of other elements or the occurrence of heat treatments which produce negligible effects on E but can strongly affects the strength characteristics (σ_0 and n).

The present method can also be extended to other materials by enlarging the database to other classes of alloys. Indeed, the verified capability of the method to represent several materials having strongly different properties (form Al and Cu alloys with either high or low ductility up to stiff and strong steels) indicates that the extension to other classes should not induce particular problems.

On the contrary, on the authors opinion, the extension of the method to more complex σ–ε curves is not so simple. In fact, as already mentioned, a linear strain hardening could be considered instead of the Hollomon power expression. The problem can arise if an expression with more than three parameters is used.

In this case, the dimension of the database increases with the corresponding number of the FE simulations. Moreover, the direct procedure becomes more difficult to be defined and obtained. The interpolating functions (6) A_k should be defined in a three-dimensional domain thus making not simple the choice of the proper expansions to fit the FE solutions. However, the main problem would appear when applying the inverse procedure. If the number of parameters increases, the efficiency and the convergence of the optimization algorithm could be no more guaranteed. With a σ–ε curve defined by more than three parameters, similar σ–ε curves could be produced by different combinations of parameters and this can produce instability and non-convergence in the inverse procedure.

It is worth noting that, in spite of the accuracy of the measurement and of the elaboration, the spherical indentation is a rather indirect method for getting the σ–ε properties. For this reason, on the authors' opinion, the evaluation of the three main characteristics of the uniaxial curve (that are indeed: E, σ_0 and n) are the only quantities that can be deduced from this test with reasonable reliability.

6. Conclusions

The satisfactory general agreement between the effective and calculated stress–strain curves for many materials having different mechanical properties confirms the validity of the whole method that can be proposed as an effective experimental tool for testing metallic materials.

In particular, an extensive finite element modelling of the indentation process gave an accurate reproduction of the load vs. penetration depth curves (L–h), allowing to distinguish the material response as a function of elastic and elastic–plastic properties.

On the basis of these results a database of L–h curves was build up covering the whole range of properties for three classes of metallic materials: steels, Cu-alloys and Al-alloys. A Hollomon's law was adopted to represent the σ–ε curve. In this way, a direct procedure was set up by which any L–h curve can be obtained on the basis of the Young modulus (E) the limit of proportionality stress (σ_0) and the strain-hardening coefficient (n).

An inverse procedure, starting from experimentally measured pairs of load and depth of penetration, was developed for deducing the σ–ε curve by means of an optimization algorithm. The inverse procedure was validated by analyzing several experimental L–h curves. The Hollomon representation produced by the inverse procedure fits the experimental points with an accuracy comparable to that of a direct interpolation by the Hollomon curve.

For the practical application of the procedure, the authors can produce the σ–ε curve on the basis of L–h data provided by any reader along with experimental details.

References

Au, P., Lucas, G.E., Sheckerd, J.W., Odette, G.R., 1980. Flow property measurements from instrumented hardness Tests. In: Non-Destructive Evaluation in the Nuclear Industry, vol. 10. ASM, New York, pp. 597–610.

Beghini, M., Bertini, L., Carsughi, F., Rosellini, W., 2001. Mechanical characterization of metallic materials by shear punch tests. In: Proceedings of the XXX Convegno Nazionale dell'Associazione Italiana per l'Analisi delle Sollecitazioni. Alghero, Italy, 12–15 September 2001, pp. 657–666 (in Italian).

Beghini, M., Bertini, L., Fontanari, V., 2002. On the possibility to obtain the stress–strain curve for a strain-hardening material by spherical indentation. Int. J. Computer Appl. Technol. 15 (4/5), 168–175.

Field, J.S., Swain, M.V., 1993. A simple predictive model for spherical indentation. J. Mater. Res. 8 (2), 297–306.

Fischer-Cripps, A.C., 1997. Elastic–plastic behaviour in materials loaded with a spherical indenter. J. Mater. Sci. 32, 727–736.

Fischer-Cripps, A.C., 2000. Introduction to Contact Mechanics. Mechanical Engineering Series. Springer Verlag, New York.

Francis, H.A., 1976. Phenomenological analysis of plastic spherical indentation. J. Eng. Mater. Tech. Trans., ASME, 272–281.

Giannakopoulos, A.E., Suresh, S., 1999. Determination of elastoplastic properties by instrumented sharp indentation. Scr. Mater. 40 (10), 1191–1198.

Herbert, E.G., Pharr, G.M., Oliver, W.C., Lucas, B.N., Hay, J.L., 2001. On the measurements of stress–strain curves by spherical indentation. Thin solid films 398–399, 331–335.

Hill, R., Storakers, B., Zdunek, A.B., 1989. A theoretical study of the Brinnel hardness test. Proc. R. Soc. Lond. A 436, 301–330.

Huber, N., Munz, D., Tsamakis, Ch., 1997. Determination of Young modulus by spherical indentation. J. Mater. Res. 12 (9), 2459–2469.

Johnson, K.L., 1985. Contact Mechanics. Cambridge University Press, Cambridge, pp. 171–179.

Lai, M.O., Lim, K.B., 1991. On the prediction of tensile properties from hardness tests. J. Mater. Sci. 26, 2031–2036.

Matthews, J.R., 1980. Indentation hardness and hot pressing. Acta Metall. 28, 311–318.

Mesarovic, S.D., Fleck, N.A., 1999. Spherical indentation of elastic–plastic solids. Proc. R. Soc. Lond. A 455, 2707–2728.

Meyer, E., 1908. Untersuchungen über Härteprufung und Härte. Z. Ver. Deutsche Ing. 52, 645–654.

Nayebi, A., Bartier, O., Mauvoisin, G., El Abdi, R., 2001. New method to determine the mechanical properties of heat treated steels. Int. J. Mech. Sci. 43, 2679–2697.

Nayebi, A., El Abdi, R., Bartier, O., Mauvoisin, G., 2002. New procedure to determine steel mechanical parameters from the spherical indentation technique. Mech. Mater. 34, 243–254.

Norbury, A.L., Samuel, T., 1928. The recovery and sinking in or piling up of material in the Brinell test and the effects of these factors on the correlation of the Brinell with other hardness tests. J. Iron Steel Inst. 117, 673–675.

Pharr, G.M., Oliver, W.C., 1992. An improved technique for determining hardness and elastic modulus using load and displacement sensing indentation experiments. J. Mater. Res. 7 (6), 1564–1583.

Pharr, G.M., Oliver, W.C., Brotzen, F.R., 1992. On the generality of the relationship among contact stiffness, contact area and elastic modulus during indentation. J. Mater. Res. 7 (3), 613–617.

Rickerby, D.G., 1982. Elastic recovery in spherical indentations. Mater. Sci. Eng. 56, 195–201.

Shabel, B.S., Young, R.F., 1987. A new procedure for the rapid determination of yield and tensile strength from hardness tests. In: Bussiere, J.F. (Ed.), Nondestructive Characterization of Materials II. Plenum Press, New York, pp. 335–343.

Tabor, D., 1951. The Hardness of Metals. Clarendon Press, London.

Taljat, B., Zacharia, T., Kosel, F., 1998. New analytical procedure to determine stress–strain curve from spherical indentation data. Int. J. Solids Struct. 35 (33), 4411–4426.

Tirupataiah, Y., Sundararajan, G., 1991. On the constraint factor associated with the indentation of work hardening materials. Metall. Trans. A 22, 2375–2384.